Automated quantification of floating wood pieces in rivers from video monitoring: a new software tool and validation.

Hossein Ghaffarian[1, *,] Pierre Lemaire[1,2], Zhang Zhi[1], Laure Tougne[2], Bruce MacVicar[3], and Hervé Piégay[1]

[1]Univ. Lyon, UMR 5600, Environnement-Ville-Société CNRS, F-69362 Lyon, France
[2]Univ. Lyon, UMR 5205, Laboratoire d'InfoRmatique en Image et Systèmes d'information CNRS, F-69676 Lyon, France
[3]Department of Civil and Environmental Engineering, Univ. Waterloo, Waterloo, Ontario, Canada

Correspondence to: Hossein Ghaffarian (hossein.ghaffarian@ens-lyon.fr)

Abstract

Wood is an essential component of rivers and plays a significant role in ecology and morphology. It can be also considered as a risk factor in rivers due to its influence on erosion and flooding. Quantifying and characterizing wood fluxes in rivers during floods would improve our understanding of the key processes but is hindered by technical challenges. Among various techniques for monitoring wood in rivers, streamside videography is a powerful approach to quantify different characteristics of wood in rivers, but past research has employed a manual approach that has many limitations. In this work, we introduce new software for the automatic detection of wood pieces in rivers. We apply different image analysis techniques such as static and dynamic masks, object tracking, and object characterization to minimize false positive and missed detections. To assess the software performance, results are compared with manual detections of wood from the same videos, which was a time-consuming process. Key parameters that affect detection are assessed including surface reflections, lighting conditions, flow discharge, wood position relative to the camera, and the length of wood pieces. Preliminary results had a 36% rate of false positive detection, primarily due to light reflection and water waves, but post-processing reduced this rate to 15%. The missed detection rate was 71% of piece numbers in the preliminary result, but post processing reduced this error to only 6.5% of piece numbers, and 13.5% of volume. The high precision of the software shows that it can be used to massively increase the quantity of wood flux data in rivers around the world, potentially in real time. The significant impact of post-processing indicates that it is necessary to train the software in various situations (location, timespan, weather conditions) to ensure reliable results. Manual wood detections and annotations for this work took over 150 labor-hours. In comparison, the presented software coupled with an appropriate post processing step performed the same task in real time (55 hr) on a standard desktop computer.

30   Keywords: River monitoring, Wood flux, Wood discharge, Large wood, Ground video imagery, Auto-
31   matic detection

1.   Introduction

33   Floating wood has a significant impact on river morphology (Gurnell et al., 2002; Gregory et al., 2003;
34   Wohl, 2013; Wohl and Scott, 2017). It is both a component of stream ecosystems and a source of risk for
35   human activities (Comiti et al., 2006; Badoux et al., 2014; Lucía et al., 2015). The deposition of wood at
36   given locations can cause a reduction of the cross-sectional area, which can both increase upstream water
37   levels (and the risk for neighboring communities), and laterally concentrate the flow downstream, which can
38   lead to damaged infrastructure (Lyn et al., 2003; Lagasse, 2010; Mao and Comiti, 2010; Badoux et al., 2014;
39   Ruiz-Villanueva et al., 2014; De Cicco et al., 2018; Mazzorana et al., 2018). Therefore, understanding and
40   monitoring the dynamics of wood within a river is fundamental to assess and mitigate risk. An important
41   body of work on this topic has grown over the last two decades, which has led to the development of many
42   monitoring techniques (Marcus et al., 2002; MacVicar et al., 2009a; MacVicar and Piégay, 2012; Benacchio
43   et al., 2015; Ravazzolo et al., 2015; Ruiz-Villanueva et al., 2019; Ghaffarian et al., 2020; Zhang et al., 2021)
44   and conceptual and quantitative models (Braudrick and Grant, 2000; Martin and Benda, 2001; Abbe and
45   Montgomery, 2003; Gregory et al., 2003; Seo and Nakamura, 2009; Seo et al., 2010). A recent review by
46   Ruiz-Villanueva et al. (2016), however, argues that the area remains in relative infancy compared to other
47   river processes such as the characterization of channel hydraulics and sediment transport. Many questions
48   remain open areas of inquiry including wood hydraulics, which is needed to understand wood recruitment,
49   movement and trapping, and wood budgeting, where better parametrization is needed to understand and
50   model the transfer of wood in watersheds at different scales.

51   In this domain, the quantification of wood mobility and wood fluxes in real rivers is a fundamental
52   limitation that constrains model development. Most early works were based on repeated field surveys (Keller
53   and Swanson, 1979; Lienkaemper and Swanson, 1987), with more recent efforts taking advantage of aerial
54   photos or satellite images (Marcus et al., 2003; Lejot et al., 2007; Lassettre et al., 2008; Senter and Pasternack,
55   2011; Boivin et al., 2017) to estimate wood delivery at larger time scales of 1 year up to several decades.
56   Others have monitored wood mobility once introduced by tracking wood movement in floods (Jacobson et
57   al., 1999; Haga et al., 2002; Warren and Kraft, 2008). Tracking technologies such as active and passive Radio
58   Frequency Identification transponders (MacVicar et al., 2009a; Schenk et al., 2014) or GPS emitters and

59 receivers (Ravazzolo et al., 2015) can improve the precision of this strategy. To better understand wood flux,

60 specific trapping structures such as reservoirs or hydropower dams can be used to sample the flux over time

61 interval windows (Moulin and Piégay, 2004; Seo et al., 2008; Turowski et al., 2013). Accumulations up-

62 stream of a retention structure can also be monitored where they trap most or all of the transported wood, as

63 was observed by Boivin *et al.* (2015), to quantify wood flux at the flood event or annual scale. All these

64 approaches allow the assessment of wood budget and the in-channel wood exchange between geographical

65 compartments within a given river reach and over a given period (Schenk et al., 2014; Boivin et al., 2015,

66 2017).

67 For finer scale information on the transport of wood during flood events, video recording of the water

68 surface is suitable for estimating instantaneous fluxes and size distributions of floating wood in transport

69 (Ghaffarian et al., 2020). Classic monitoring cameras installed on the river bank are cheap and relatively easy

70 to acquire, setup and maintain. As is seen in Table 1, a wide range of sampling rates and spatial/temporal

71 scales have been used to assess wood budgets in rivers. MacVicar and Piégay (2012) and Zhang et al. (2021)

72 (in review), for instance, monitored wood fluxes at 5 frames per second (fps) and a resolution of 640×480

73 up to 800×600 pixels. Boivin et al. (2017) used a similar camera and frame rate as MacVicar and Piégay

74 (2012) to compare periods of wood transport with and without the presence of ice. Senter et al. (2017) ana-

75 lyzed the complete daytime record of 39 days of videos recorded at 4 fps and a resolution of 2048×1536

76 pixels. Conceptually similar to the video technique, time-lapse imagery can be substituted when large rivers

77 where surface velocities are low enough and the field of view is large. Kramer and Wohl (2014); Kramer et

78 al. (2017) applied this technique in the Slave River (Canada) and recorded one image every 1 and 10 minutes.

79 Where possible, wood pieces within the field of view are then visually detected and measured using simple

80 software to measure the length and diameter of the wood to estimate wood flux (piece/s) or wood volume

81 (m^3/s) (MacVicar and Piégay, 2012; Senter et al., 2017). Critically for this approach, the time it takes for

82 the researchers to extract information about wood fluxes has limited the fraction of the time that can be

83 reasonably analyzed. Given the outdoor location for the camera, the image properties depend heavily on

84 lighting conditions (e.g. surface light reflections, low light, ice, poor resolution or surface waves) which may

85 also limit the accuracy of frequency and size information (Muste et al., 2008; MacVicar et al., 2009a). In

86 such situations, simpler metrics such as a count of wood pieces, a classification of wood transport intensity,

87 or even just a binary presence/absence may be used to characterize the wood flux (Boivin et al., 2017; Kramer

88 et al., 2017).

Table 1 Characteristics of streamside video monitoring techniques in different studies.

Article	Sampling	Temporal scales	Camera resolution	Study site
MacVicar & Piégay (2012)	15 min segments	3 floods/18 hr/5 fps	640×480	Ain, France
Kramer & Wohl (2014)	Total duration	32 days/12761 frames/0.017 fps	n/a	Slave, Canada
Boivin et al. (2017)	Total duration	3 floods/150 hr/25 fps	640×480	St Jean, Canada
Kramer et al. (2017)	Total duration	11 months/0.0017 fps	1268×760	Slave, Canada
Senter et al. (2017)	15 min segments	39 days/180 hr/4 fps	2048×1536	North Yuba, USA
Ghaffarian et al. (2020)	Total duration	2 floods/80 hr/1 fps	600×800	Isère, France
Zhang et al.(2021)	Total duration	7 floods & 1 windy period /183 hr/5 fps	from 640×480 up to 800×600	Ain, France

89   A fully automatic wood detection and characterization algorithm can greatly improve our ability to
90 exploit the vast amounts of data on wood transport that can be collected from streamside video cameras.
91 From a computer science perspective, however, automatic detection and characterization remain challenging
92 issues. In computer vision, detecting objects within videos typically consists of separating the foreground
93 (the object of interest) from the background (Roussillon et al., 2009; Cerutti et al., 2011, 2013). The basic
94 hypothesis is that the background is relatively static and covers a large part of the image, allowing it to be
95 matched between successive images. In the riverine environments, however, such an assumption is unrealistic
96 because the background shows a flowing river, which can have rapidly fluctuating properties (Ali and
97 Tougne, 2009). Floating objects are also partially submerged in water that has high suspended material con-
98 centrations during floods, making them only partially visible (*e.g.* a single piece of wood may be perceived
99 as multiple objects) (MacVicar et al., 2009b). Detecting such an object in motion within a dynamic back-
100 ground is an area of active research (Ali et al., 2012, 2014; Lemaire et al., 2014; Piégay et al., 2014; Be-
101 nacchio et al., 2017). Accurate object detection typically relies on the assumption that objects of a single
102 class (e.g., faces, bicycles, animals, etc.) have a distinctive aspect or set of features that can be used to dis-
103 tinguish between types of objects. With the help of a representative dataset, machine learning algorithms aim
104 at defining the most salient visual characteristics of the class of interest (Lemaire et al., 2014; Viola and
105 Jones, 2006). When the objects have a wide intra-class aspect range, a large amount of data can compensate
106 by allowing the application of deep learning algorithms (Gordo et al., 2016; Liu et al., 2020). To our
107 knowledge, such a database is not available in the case of floating wood.

108   The camera installed on the Ain River in France has been operating more or less continuously for over
109 10 years and vast improvements in data storage mean that this data can be saved indefinitely (Zhang et al.,
110 2021). The ability to process this image database to extract the wood fluxes allows us to integrate this

111   information over floods, seasons and years, which would allow us to significantly advance our understanding

112   of the variability within and between floods over a long time period. An unsupervised method to identify

113   floating wood in these videos by applying intensity, gradient and temporal masks was developed by Ali and

114   Tougne (2009) and Ali et al. (2011). In this model, the objects were tracked through the frame to ensure that

115   they followed the direction of flow. An analysis of about 35 minutes of the video showed that approximately

116   90% of the wood pieces was detected (*i.e.,* about 10% of detection were missed), which confirmed the po-

117   tential utility of this approach. An additional set of false detection related to surface wave conditions

118   amounted to approximately 15% of the total detection. However, the developed algorithm was not always

119   stable and was found to perform poorly when applied to a larger data set (i.e., Video segments more than

120   1hr).

121   The objectives of the presented work are to describe and validate a new algorithm and computer inter-

122   face for quantifying floating wood pieces in rivers. First, the algorithm procedure is introduced to show how

123   wood pieces are detected and characterized. Second, the computer interface is presented to show how manual

124   annotation is integrated with the algorithm to train the detection procedure. Third, the procedure is validated

125   using data from the Ain River. The validation period occurred over six days in January and December 2012

126   where flow conditions ranged from $\sim400\ m^3/s$, which is below bankfull discharge but above the wood

127   transport threshold, to more than $800\ m^3/s$.

2.   Monitoring site and camera settings

129   The Ain River is a piedmont river with a drainage area of $3630\ km^2$ at the gauging station of Chazey-

130   sur-Ain, with a mean flow width of 65 m, a mean slope of 0.15%, and a mean annual discharge of $120\ m^3/s$.

131   The lower Ain River is characterized by an active channel shifting within a forested floodplain (Lassettre et

132   al., 2008). An AXIS221 Day/Night^{TM} camera with a resolution of 768×576 pixels was installed at this station

133   to continuously record the water surface of the river at a maximum frequency of 5 fps (Fig 1). This camera

134   replaced a lower resolution camera at the same location used by MacVicar and Piégay (2012). The specific

135   location of the camera is on the outer bank of a meander, on the side closest to the thalweg, at a height of 9.8

136   m above the base flow elevation. The meander and a bridge pier upstream help to steer most of the floating

137   wood so that it passes relatively close to the camera where it can be readily detected with a manual procedure

138   (MacVicar and Piégay, 2012). The flow discharge is available from the website (*www.hydro.eaufrance.fr*).

139   The survey period examined on this river was during 2012 from which two flood events, (January 1-7

140   and December 15) were selected for annotation. A range of discharges from $400 m^3/s$ to $800\ m^3/s$ occurred

141   during these periods (Fig 1.e), which is above a previously observed wood transport threshold of $\sim 300\ m^3/s$

142   (MacVicar and Piégay, 2012). A summary of automated and manual detections for the six days is shown in

143   Table 3.

144
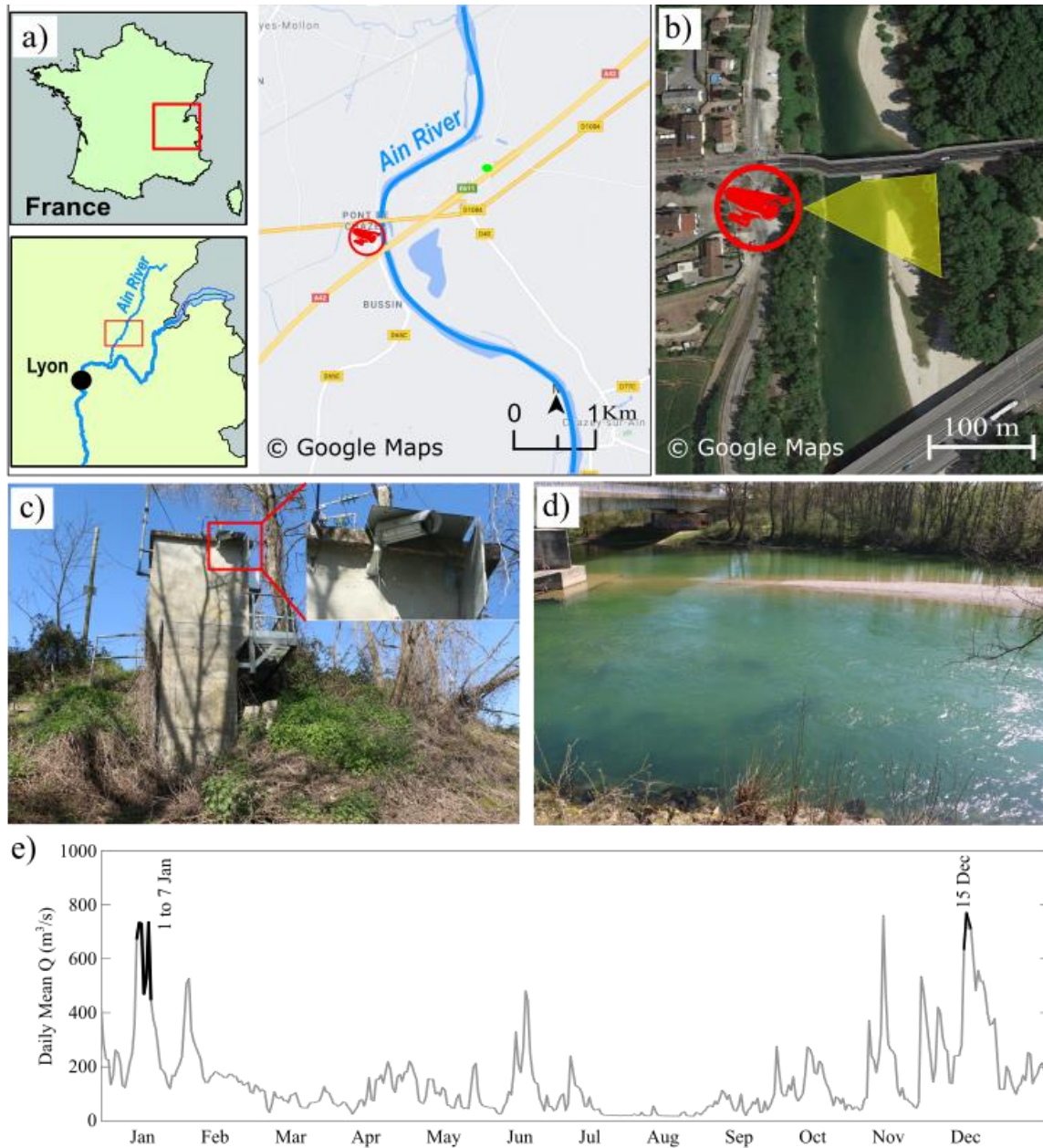
Fig 1 Study site at Pont de Chazey: a) Location of the Ain River catchment in France and location of the gauging station, b) camera position and its view angle in yellow, c) overview of the gauging station with the camera installation point, and d) view of the River channel from the camera. e) Daily mean discharge series for monitoring period from 1st to 7th January and in 15th December.

3.   Methodological procedure for automatic detection of wood

145

146   The algorithm for wood detection comprises a number of steps that seek to locate objects moving

147   through the field of view in a series of images and then identify the objects most likely to be wood. The

148   algorithm used in this work modifies the approach described by Ali et al. (2011). The steps work from a pixel

149   to image to video scale, with the context from the larger scale helping to assess whether the information at

150   the smaller scale indicates the presence of floating wood or not. In a still image, a single pixel is characterized

151   by its location within the image, its color and its intensity. Looking at its surrounding pixels, on an image

152   scale, allows that information to be spatially contextualized. Meanwhile, the video data adds temporal con-

153   text, so that previous and future states of a given pixel can be used to assess its likeliness of representing

154   floating wood. On a video scale, the method can embed expectations about how wood pieces should move

155   through frames, how big they should be, and how lighting and weather conditions can evolve to change the

156   expectations of wood appearance, location, and movement. The specific steps followed by the algorithm are

157   shown in a simple flow chart (Fig 2.a). An example image with a wood piece in the middle of the frame is

158   also shown for reference (Fig 2.b).
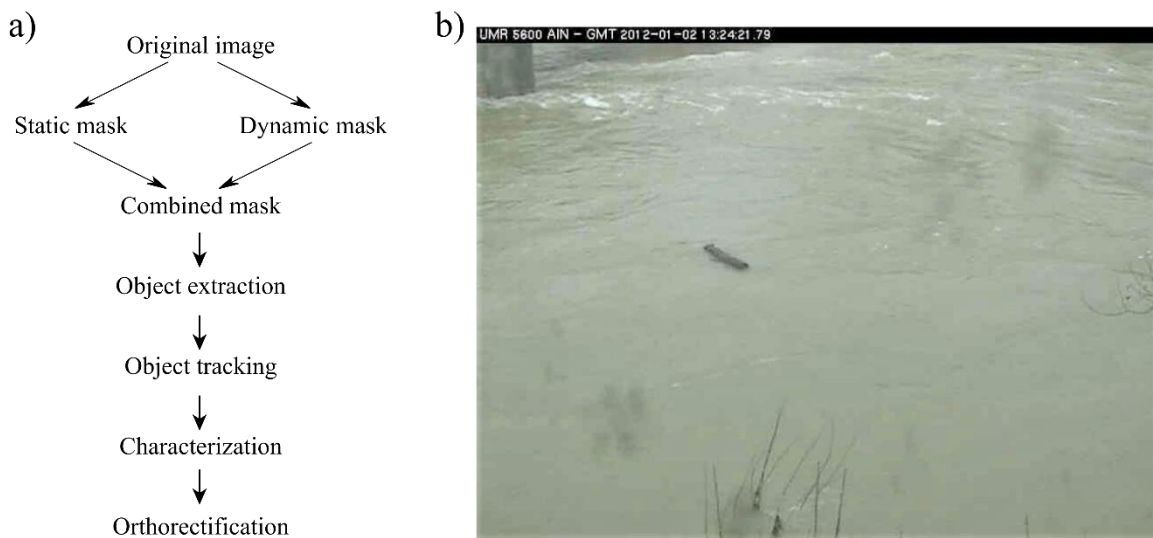
159

Fig 2 a) Flowchart of the detection software and b) an example of frame on which these different flowchart steps are applied.

3.1. Wood probability masks

160

161   In the first step, each pixel was analyzed individually and independently. The static probability mask

162   answers the question "is one pixel likely to belong to a wood-block, given its color and intensity?". The

163   algorithm assumes that the wood pixels can be identified by pixel light intensity (i) following a Gaussian

164   distribution (Fig 3.a). To set the algorithm parameters, pixelwise annotations of wood under all the observed

165   lighting conditions were used to determine the mean (μ) and standard deviation (σ) of wood piece pixel

166   intensity. Applying this algorithm produces a static probability mask (Fig 3.b). From this figure, it is possible

167   to identify the sectors where wood presence is likely, which includes the floating wood piece seen in Fig 2.b,

168   but also includes standing vegetation in the lower part of the image and a shadowed area in the upper left.

169   The advantage of this approach is that it is computationally very fast. However, misclassification is possible,

170   particularly when light condition changes.
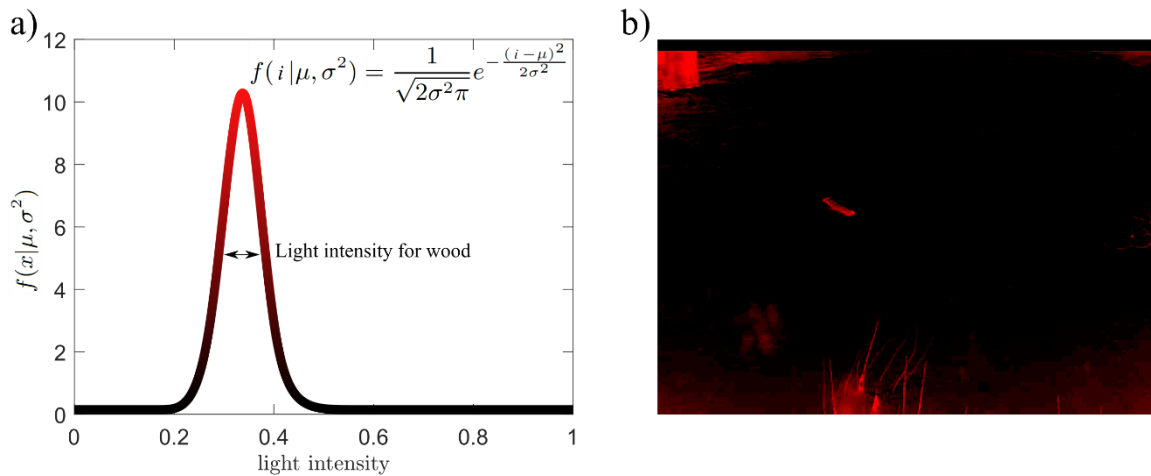
171

Fig 3 Static probability mask, a) Gaussian distribution of light intensity range for a piece of wood, b) employment of probability mask on the sample frame.

172   The second mask, called the dynamic probability mask, outlines each pixel's recent history. The corre-

173   sponding question is: "is this pixel likely to represent wood now, given its past and present characteristics?".

174   Again, this step is based on what is most common in our database: it is assumed that a wood pixel is darker

175   than a water pixel. Depending on lighting conditions like shadows cast on water or waves, this is not always

176   true, i.e., water pixels can be as dark as wood pixels. However, pixels displaying successively water than

177   wood tend to become immediately and significantly darker, while pixels displaying wood then water tend to

178   become significantly lighter. Meanwhile, the intensity of pixels that keep on displaying wood tends to be

179   rather stable. Thus, we assign wood pixel probability according to an updated version of the function pro-

180   posed by Ali et al. (2011) (Fig 4.a) that takes 4 parameters. This function H is an updating function, which

181   produces a temporal probability mask from the inter-frame pixel value. On a probability map, a pixel value

182   ranges from -1 (likely not wood) to 1 (likely wood). The temporal mask value for a pixel at location (x, y)

183 and at time t is $P_T(x, y, t) = H(\Delta_t, I) + P_T(x, y, t - 1)$. We apply a threshold to the output of $P_T(x, y, t)$ so

184 that it always stays within the interval $[0,1]$. The idea is that a pixel that becomes suddenly and significantly

185 darker is assumed to be likely wood. $H(\Delta_t, I)$ is such that under those conditions, it increases the pixel prob-

186 ability map value (parameters τ and β). A pixel that becomes lighter over time is unlikely to correspond to

187 wood (parameter α). A pixel which intensity is stable and that was previously assumed to be wood shall still

188 correspond to wood, while a pixel which intensity is stable and which probability to be wood was low is

189 unlikely to represent wood now. A small decay factor (δ) was introduced in order to prevent divergence (in

190 particular, it prevents noisy areas from being activated too frequently).
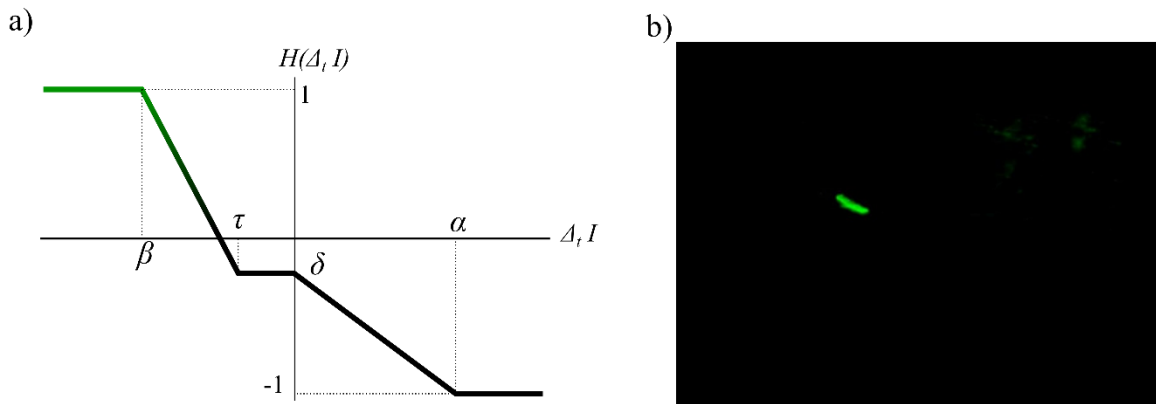
191

Fig 4 Dynamic probability mask, a) updating function $H(\Delta_t, I)$ adapted from Ali et al. (2011) and b) employment of probability mask on the sample frame.

192 The final wood probability mask is created using a combination of both the static and dynamic proba-

193 bility masks. Wood objects thus had to have a combination of the correct pixel color and the expected tem-

194 poral behavior of water-wood-water color. The masks were combined assuming that both probabilities are

195 independent, which allowed us to use the Bayesian probability rule in which the probability masks are simply

196 multiplied, pixel by pixel, to obtain the final probability value for each pixel of every frame.

197 **3.2. Wood object identification and characterization**

198 From the probability mask it is necessary to group pixels with high wood probabilities into objects and

199 then to separate these objects from the background to track them through the image frame. For this purpose,

200 pixels were classified as high-or low-probability based on a threshold applied to the combined probability

201 mask. Then, the high-probability pixels were grouped into connected components (that is, small, contiguous

202 regions on the image) to define the objects. At this stage, a pixel size threshold was applied on the detected

203 objects so that only the bigger objects were considered to represent woody objects on the water surface (Fig
204 5.a the big white region at the middle). A number of smaller components were often related to non-wood
205 objects, for example waves, reflections, or noise from the camera sensor or data compression.

206 After the size thresholding step, movement direction and velocity were used as filters to distinguish real
207 objects from false detections. The question here is, "is this object moving through the image frame the way
208 we would expect floating wood to move?". To do this, the spatial and temporal behavior of components were
209 analyzed. First, to deal with partly immersed objects, we agglomerated multiple objects within frames as
210 components of a single object if the distance separating them was less than a set threshold. Second, we asso-
211 ciated wood objects in successive frames together to determine if the motion of a given object was compatible
212 with what is expected from driftwood. This can be achieved according to the dimensionless parameter
213 "$PT/\Delta T$", which provides a general guideline for the distance an object pass between two consecutive frames
214 (Zhang et al., 2021). Here PT (passing time) is the time that one piece of wood passes through the camera
215 field of view and ΔT is the time between two consecutive frames and practically it is recommended to use
216 videos with $PT/\Delta T > 5$ in this software. In our case, tracking wood is rather difficult for classical object
217 tracking approaches in computer vision: the background is very noisy, the acquisition frequency is low and
218 the objects appearance can be highly variable due to temporarily submerged parts and highly variable 3D
219 structures. Given these considerations it was necessary to use very basic rules for this step. The rules are
220 therefore based on loose expectations, in terms of pixel intervals, on the motions of the objects, depending
221 on the camera location and the river properties. How many pixels is the object likely to move between image
222 frames from left to right? How many pixels from top to bottom? How many appearances are required? How
223 many frames can we miss because of temporary immersions? Using these rules, computational costs re-
224 mained low and the analysis could be run in real-time while also providing good performance.
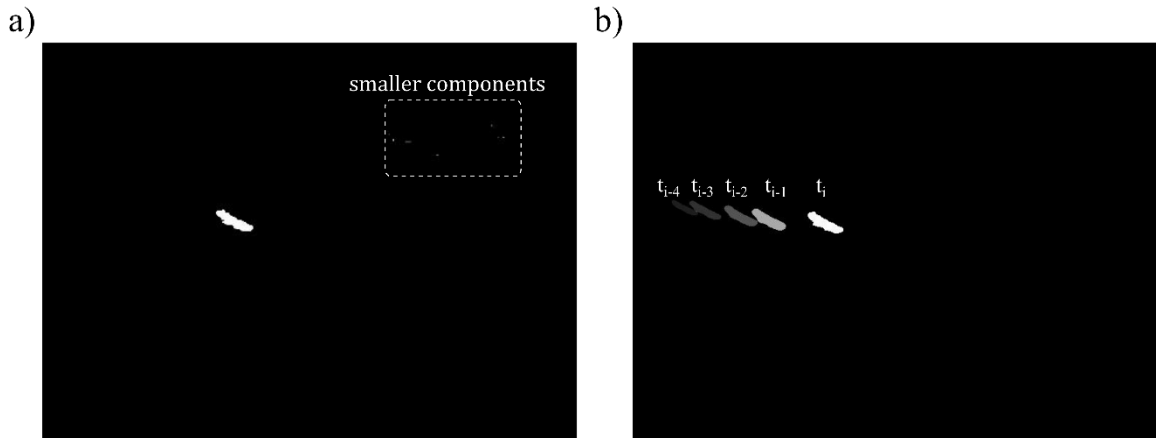
Fig 5 a) Object extraction by (i) combining static and dynamic masks and (ii) applying a threshold to retain only high-probability pixels. b) Object tracking as a filter to deal with partly immersed objects and to distinguish between moving objects from static waves.

The final step was to characterize each object, which at this point in the process are considered wood objects. Each appears several times in different frames and a procedure is needed to either pick a single representative occurrence or use a statistic tool to analyze multiple occurrences to estimate characterization data. In this step, all images containing the object are transformed from pixel to cartesian coordinates (as will be described in the next section) and the median length is calculated and used as the most representative state. This approach also matched the manual annotation procedure where we tended to pick the view where the object covers the largest area to make measurements. For the current paper, every object as characterized from the raw image based on its size and its location. It is worth to say detection was only possible during the daylight.

3.3. Image rectification

Warping images according to a perspective transform results in an important loss of quality. On warped images, areas of the image farther from the camera provide little detail and are overall very blurry and non-informative. Therefore, image rectification was necessary to calculate wood length, velocity, and volume from the saved pixel-based characterization of each object. To do so, the fisheye lens distortion was first corrected. A fisheye lens distortion is a characteristic of the lens that produces visual distortion intended to create a wide panoramic or hemispherical image. This effect was corrected by a standard Matlab process using the ComputerVisionToolbox™ (Release 2017b).

Ground-based cameras have also an oblique angle of view, which means that pixel to meter

correspondence is variable and images need to be orthorectified to obtain estimates of object size and velocity
in real terms (Muste et al., 2008). Orthorectification refers to the process by which image distortion is re-
moved and the image scale is adjusted to match the actual scale of the water surface. Translating from pixels
to cartesian coordinates required us to assume that our camera follows the pinhole camera model and that the
river can be assimilated to a plane of constant altitude. Under such conditions, it is possible to translate from
pixel coordinates to a metric 2D space thanks to a perspective transform assuming a virtual pinhole camera
on the image and estimating the position of the camera and its principal point (center of the view). An exam-
ple of orthorectification on a detected wood piece in a set of continuous frames and pixel coordinates (Fig
6.a) is presented in Fig 6.b in metrics coordinates. The transform matrix is obtained with the help of at least
4 non-colinear points (Fig 6.c blue GCPs (Ground Control Points) acquired with DGPS) from which we
know both the relative 2D metric coordinates for a given water level (Fig 6.b blue points), and their corre-
sponding localization within the image(Fig 6.a blue points). To achieve better accuracy, it is advised to ac-
quire additional points and to solve the subsequent over-determined system with the help of a Least Square
Regression (LSR). Robust estimators such as RANSAC (Forsyth and Ponce, 2012) can be useful tools to
prevent acquisition noise. After identifying the virtual camera position, the perspective transform matrix then
becomes parameterized with the water level. Handling the variable water level was performed for each piece
of wood, by measuring the relative height between the camera and the water level at the time of detection
based on information recorded at the gauging station to which the camera was attached. The transformation
matrix on the Ain River at the base flow elevation with the camera as the origin is shown in Fig 6.d. Straight
lines near the edges of the image appear curved because the fisheye distortion has been corrected on this
image; conversely, a straight line, in reality, is presented without any curvature in the image.
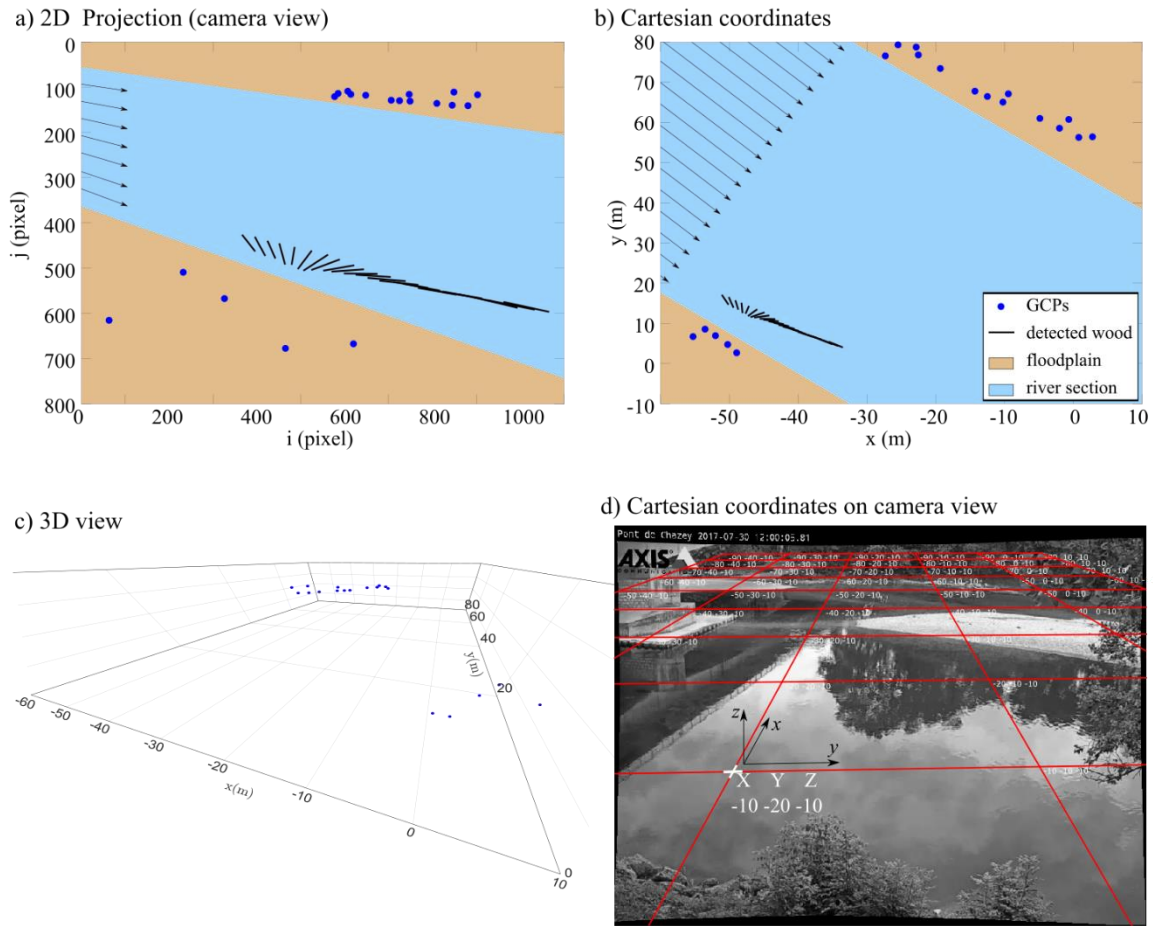
265

Fig 6 Image rectification, process. The non-colinear GCPs localization within the image (a), and the relative 2D metric coordinates for a given water level (b). The different solid lines represent the successive detection in a set of consecutive frames. (c) 3D view of non-colinear GCPs in metric coordinates. (d) Rectifying transformation matrix on the Ain River at low flow level with camera at (0,0,0).

266 **4.   User interface**

267   The software was developed to provide a single environment for the analysis of wood pieces on the

268   surface of the water from streamside videos. It consists of four distinct modules: Detection, Annotation,

269   Training, and Performance. The home screen allows the operator to select any of these modules. From within

270   a module, a menu bar on the left side of the interface allows operators to switch from one module to another.

271   In the following sections, the operation of each of these modules are described.

4.1. Detection module

The detection module is the heart of the software. This module allows, from learned or manually specified parameters, the detecting of floating objects without human intervention (see Fig 7). This module contains two main parts: (i) Detection tab, which allows operator to open, analyze and export the results from one video or a set of videos, and (ii) Configuration tab, which allows operator to load and save the software configuration by defining the parameters of wood detection (as described in Sect 3), saving and extracting the results, and displaying the interface.

The detection process works as a video file player. The video file (or a stream url) is loaded, and to let the software read the video until the end. When required, the reader generates a visual output, showing how the masks behave by adding color and information to the video content (see Fig 7.a). A small textual display area shows the frequency of past detections. Meanwhile, the software generates a series of files summarizing the positive outputs of the detection. They consist in YAML and CSV files, as well as image files to show the output of different masks, the original frames, etc. A configuration tab is available, and provides many parameters organized by various categories. The main configuration tab is divided in seven parts. The first part is dedicated to general configurations such as frame skipped between each computation and defining the areas within the frame where wood is not expected (e.g., bridge pier or river bank). In the second and third parts, the parameters of the intensity and temporal masks are listed (see Sect 3.1). The default values are $\mu = 0.2$ and $\sigma = 0.08$ for the intensity mask, and $\tau = 0.25$ and $\beta = 0.45$ for the temporal mask. In the fourth and fifth parts, object tracking and characterization parameters are defined respectively as described in Sect 3.2. Detection time is defined in the sixth part using an optical character recognition technique. Finally, the parameters of the orthorectification (see Sect 3.3) are defined in the seventh part. The detection software can be used to process videos in batch ("script" tab), without generating a visual output to save computing resources.
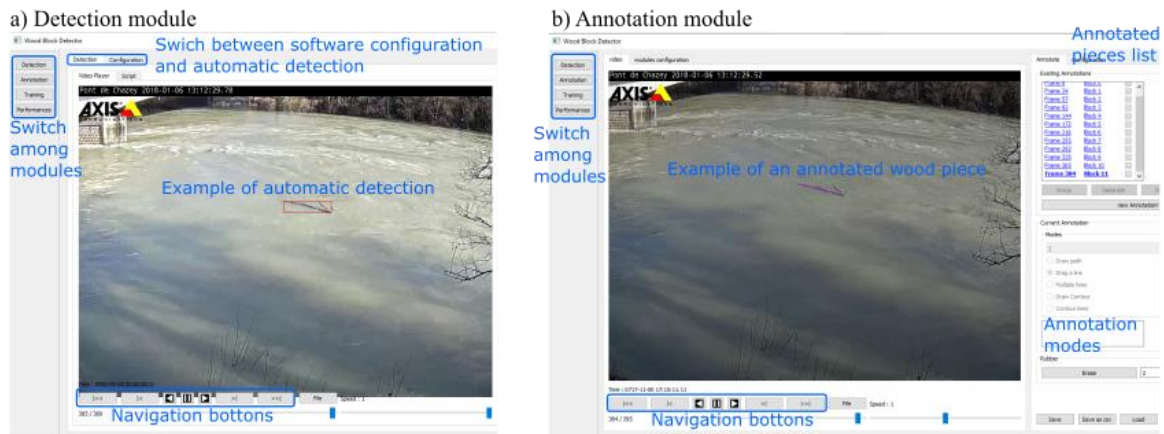
Fig 7 User interface of (a) detection module and (b) annotation module of automatic detection software.

4.2. Annotation module

As mentioned in Sec. 2, the detection procedure requires the classification of pixels and objects into wood and non-wood categories. To train and validate the automatic detection process, a ground-truth or set of videos with manual annotations are required. Such annotations can be performed using different techniques. For example, objects can be identified with the help of a bounding box or selection of endpoints, as in MacVicar and Piégay(2012); Ghaffarian et al. (2020) and Zhang et al. (2021). It is also possible to sample wood pixels without specifying instances or objects, or to sample pixels within annotated objects. Finally, objects and/or pixels can be annotated multiple times in a video sequence to increase the amount and detail of information in such an annotation database. This annotation process is time-consuming, so a trade-off must be made regarding the purpose of the annotated database and its required accuracy. Manual annotations are especially important when it is intended to be used within a training procedure, for which different lighting conditions, camera parameters, wood properties, and river hydraulics must be balanced. The rationale for manual annotations in the current study is presented in section 5.1.

Given that the tool is meant to be as flexible as possible, the annotation module was developed to allow operator to perform annotation in different ways, depending on the purpose of the study. As shown in Fig 7.b, this module contains three main parts: (i) The column on the far left allows the operator to switch to another module (detection, learning, or performance), (ii) the central part consists of a video player with a configuration tab for extracting the data, and (iii) the right part where the tools to generate, create, visualize and save annotations are located. The tools allow rather quick coarse annotation, similar to what was done by MacVicar and Piégay (2012) and Boivin et al. (2015), while still allowing the possibility of finer pixel-

316 scale annotation. The principle of this module is to associate annotations with the frames of a given video.
317 Annotating a piece of wood is like drawing its shape, directly on a frame of the video, using the drawing
318 tools provided by the module. It is possible to add a text description to each annotation. Each annotation is
319 linked to a single frame of the video; however, a frame can contain several annotations. An annotated video,
320 therefore, consists of a video file, as well as a collection of drawings, possibly with textual descriptions,
321 associated with frames. It is possible to link annotations from one frame to another to signify that they belong
322 to the same piece of wood. These data can be used to learn the movement of pieces of wood in the frame.

4.3. Performance module

324 The performance module allows the operator to set rules to compare automatic and manual wood de-
325 tection results. This section also allows the operator to use a bare, pixel-based annotation or specify an or-
326 thorectification matrix to extract wood-size metrics directly from the output of an automatic detection.

327 For this module an automatic detection file is first loaded and then the result of this detection is com-
328 pared with a manual annotation for that video, if the latter is available. Comparison results are then saved in
329 the form of a summary file (*.csv format), allowing the operator to perform statistical analysis of the results
330 or the performance of the detection algorithm. A manual annotation file can only be loaded if it is associated
331 with an automatic detection result.

332 The performance of the detected algorithm can be realized on several levels:

333 • Object. The idea is to annotate one (or more) occurrences of a single object, and to operate the
334 comparison at bounding box scale. A detected object may comprehend a whole sequence of occur-
335 rences, on several frames. It is validated when only a single occurrence happens to be related to an
336 annotation. This is the minimum possible effort required to have an extensive overview of the
337 object frequency on such an annotations database. This approach can however lead us to misjudge
338 overall wrongly detected sequences as True Positives (see below), or vice-versa.
339 • Occurrence. The idea is to annotate, even roughly, every occurrence of every woody object, so that
340 the comparison can happen between bounding boxes rather than at pixel level. Every occurrence
341 of any detected object can be validated individually. This option requires substantially more anno-
342 tation work than the object annotation.
343 • Pixel. This case implies that every pixel of every occurrence of every object is annotated as wood.

344   It is very powerful in the event of evaluating the algorithm performances, and eventually refining

345   its parameters with the help of some machine learning technique. However, it requires an extensive

346   annotation work.

347 **5. Performance assessment**

348 **5.1. Assessment procedure**

349   To assess the performance of the automatic detection algorithm, we used a set of videos from the Ain

350 River in France that were both comprehensively manually annotated and automatically analyzed. According

351 to the data annotated by the observer, the performance of the software can be affected by different conditions:

352 (i) wood piece length, (ii) distance from the camera, (iii, iv) wood X, Y position, (v) flow discharge, (vi)

353 daylight, and (vii, viii) light and darkness of the frame (see Table 2). If for example software detects a 1 cm

354 piece at a distance of 100 m from the camera, there is a high probability that this is a false positive detection.

355 Therefore, knowing the performance of the software in different conditions, it is possible to develop some

356 rules to enhance the quality of data. The advantage of this approach is that all eight parameters introduced

357 here are accessible easily in the detection process. In this section the monitoring details and annotation meth-

358 ods are introduced before the performance of the software is evaluated by comparing the manual annotations

359 with the automatic detections.

Table 2 Parameters used to assess the performance of the software

Parameter	Rational	Metric
Piece length	Larger objects are easier to detect.	Detecting an object in pixel coordinates. Transferring coordinates to metric. Calculating length, position, and distance.
Distance	Objects closer to the camera are easier to detect.	
X position	Some particular areas of turbulent flow in the field of view	
Y position	affect detection (e.g., presence of a bridge pier).	
Discharge	Flow discharge affects water color, turbulence and the amount of wood.	Recorded water elevation data and calibrated rating curve at hydrologic station.
Time	Luminosity of the frames varies with time of day.	Time of day as indicated on top of each frame.
Dark roughness	Small spots with sharp contrast (either lighter or darker) af-	% of pixels below an intensity threshold
Light roughness	fect detection.	% of pixels above an intensity threshold

360   Ghaffarian et al. (2020), Zhang et al. (2021) show that the wood discharge (m^3 per a time interval) can

361 be measured from flux or frequency of wood objects (pieces number per a time interval). An object level

362 detection was thus sufficient for the larger goals of this research at the Ain River, which is to get a complete

363   budget of transported wood volume.

364   A comparison of annotated with automatic object detections gives rise to three options:

365   • True Positive (TP): an object is correctly detected and is recorded in both the automatic and annotated
366   database
367   • False Positive (FP): an object is incorrectly detected and is recorded only in the automatic database.
368   • False Negative (FN): an object is not detected automatically and is only recorded in the annotated data-
369   base.

370   Despite overlapping occurrences of wood objects in the two databases, the objects could vary in position
371   and size between them. For the current study we set the TP threshold as the case where either at least 50%
372   of the automatic and annotated bounding box areas were common or at least 90% of an automatic bounding
373   box area was part of its annotated counterpart.

374   In addition to the raw counts of TPs, FPs, and FNs, we defined two measures of the performances of
375   the application, where:

376   • Recall Rate (RR) is the fraction of wood objects that are automatically detected ($TP/(TP + FN)$); and
377   • Precision Rate (PR) is the fraction of detected objects that are wood ($TP/(TP + FP)$).

378   The higher the PR and the RR are, the more accurate our application is. However, both rates tend to
379   interact. For example, it is possible to design an application that displays a very high RR (which means that
380   it doesn't miss many objects), but suffers from a very low PR (it outputs a high amount of inaccurate data),
381   and vice-versa. Thus, we have to find a balance that is appropriate to each application.

382   It was well known from previous manual efforts to characterize wood pieces and develop automated
383   detection tools that it is easier to detect certain wood objects than others. In general, the ability to detect the
384   wood objects in the dynamic background of a river in flood was found to vary with the size of the wood
385   object, its position in the image frame, the flow discharge, the amount and variability of the light, interference
386   from other moving objects such as spiders, and other weather conditions such as wind and rain. In this section,
387   we describe and define the metrics that were used to understand the variability of the detection algorithm
388   performance.

389   In general, more light results in better detection. The light condition can be varied by variation of a set
390   of factors such as weather conditions or amount of sediment which is carried by the river. In any case, the
391   daylight is a factor that can change the light condition systematically, *i.e.* low light early in the morning (Fig
392   8.a), bright light at midday with potential for direct light and shadows (Fig 8.b), and low light again in the
393   evening, though different from the morning because the hue is more bluish (Fig 8.c). This effect of the time
394   of day was quantified simply by noting the time of the image, which was marked on the top of each frame of
395   the recorded videos.

396

Fig 8 Different light conditions during a) morning, b) noon and c) late afternoon, results in different frame roughness's and different detection performances. c) Wood position can highly affect the quality of detection. Pieces that are passing in front of the camera are detected much better than the pieces far from the camera.

397   Detection is also strongly affected by the frame 'roughness', defined here as the variation in light over
398   small distances in the frame. The change in light is important for the recognition of wood objects, but light
399   roughness can also occur when there is a region with relatively light pixels due to something such as reflection
400   of the surface of the water, and dark roughness can occur when there is a region with relatively dark pixels
401   due to something such as shadows from the surface water waves or surrounding vegetation. Detecting wood
402   is typically more difficult around light roughness, which results in false negatives, while the color-map of a
403   darker surface is often close to that of wood, which results in false positives. Both of these conditions can be
404   seen in Fig 8 which is highlighted in Fig 8.a. In general, the frame roughness increases in windy days or
405   when there is an obstacle in the flow, such as downstream of the bridge pier in the current case. The light
406   roughness was calculated for the current study by defining a light intensity threshold and calculating the ratio
407   of pixels of higher value among the frame. The dark roughness is calculated in the same way, but in this case
408   the pixels less than the threshold were counted. In this work thresholds equal to 0.9 and 0.4 were used for
409   light and dark roughness, respectively.

410   The oblique view of the camera means that the distance of the wood piece from the camera is another
411   important factor in detection (Fig 8.c). The effect of distance on detection interacts with wood length, *i.e.*

412 shorter pieces of wood that are not detectable near the camera may not be detectable toward the far bank due
413 to the pixel size variation (Ghaffarian et al., 2020). Moreover, if a piece of wood passes through a region
414 with high roughness (Fig 8.c) or amongst bushes or trees (Fig 8.c right hand side) it is more likely that the
415 software is unable to detect it. In our case, one day of video record could not be analyzed due to the presence
416 of a spider that moved around in front of the camera.

417   Flow discharge is another key variable in wood detection. Increasing flow discharge generally means
418 that water levels are higher, which brings wood close to the near bank of the river closer to the camera. This
419 change can make small pieces of wood more visible, but it also reduces the angle between the camera position
420 and pixels, which makes wood farther from the camera harder to see. High flows also tend to increase surface
421 waves and velocity, which can increase the roughness of the frame and lead to the wood being intermittently
422 submerged or obscured. More suspended sediment is carried during high flows which can change water sur-
423 face color and increase the opacity of the water.

424 **5.2. Detection performance**

425   Automatic detection software performance was evaluated based on the event based TP, FP, and FN
426 raw numbers and the precision (PR) and recall rates (RR) using the default parameters in the software. On
427 average, manual annotation resulted in the detection of approximately twice as many wood pieces as the
428 detection software (Table 3). Measured over all the events, RR = 29%, which indicates that many wood
429 objects were not detected by the software, while among detected objects about 36% were false detections
430 ($PR = 64\%$).

Table 3 Summary of automated and manual detections

Date	discharge (m^3/s)		Water level (m)		Detection time (hr)	Number		Precision rate%	Recall rate%
	Q_{max}	Q_{min}	h_{max}	h_{min}		annot.	det.		
1/1/2012	718	633	-7.4	-7.8	7 to 17	2282	972	77	33
2/1/2012	772	674	-7.2	-7.6	7 to 17	802	380	52	24
4/1/2012	475	423	-8.4	-8.6	7 to 17	140	158	20	22
6/1/2012	786	763	-7.2	-7.2	7 to 17	712	384	54	29
7/1/2012	462	430	-8.5	-8.6	7 to 17	117	73	40	25
15/12/2012	707	533	-7.5	-8.2	9 to 14	1296	503	72	28
Total	786	423	-7.2	-8.6	55 hr	5349	2470	64	29

431   To better understand model performance, we first tested the correlation between the factors identified

432 in the previous section by calculating each one of the eight parameters for all detections as one vector and
433 then calculating the correlation between each pair of parameters (Table 4). As shown (the bold values), the
434 pairs of dark/light roughness, length/distance and discharge/time were highly correlated ($Corr.=$
435 $0.59, 0.46, 0.37$ respectively). For this reason, they were considered together to evaluate the performance of
436 the algorithm within a given parameter space. The X/Y positions were also considered as a pair despite a
437 relatively low correlation (0.15) because they represent the position of an object. As a note, the correlation
438 between time and dark roughness is higher than discharge and time, but we used the discharge/time pair
439 because discharge has a good correlation only with time. As recommended by MacVicar and Piégay (2012),
440 wood lengths were determined on a log base 2 transformation to better compare different classes of floating
441 wood, similar to what is done for sediment sizes.

Table 4 Correlation between parameters. Values in bold show significant correlation.

	Dark roughness	Light roughness	Length	Distance	X position	Y position	Discharge	Time
Dark roughness		**0.59**	-0.02	-0.04	0.04	0.1	0	0.57
Light roughness	**0.59**		-0.03	-0.03	0.03	0.09	-0.04	0.29
Length	-0.02	-0.03		**0.46**	-0.45	-0.35	-0.02	-0.01
Distance	-0.04	-0.03	**0.46**		-1	-0.16	0.14	-0.05
X position	0.04	0.03	-0.45	-1		**0.15**	-0.15	0.05
Y position	0.1	0.09	-0.35	-0.16	**0.15**		0	0.07
Discharge	0	-0.04	-0.02	0.14	-0.15	0		**0.37**
Time	0.57	0.29	-0.01	-0.05	0.05	0.07	**0.37**	
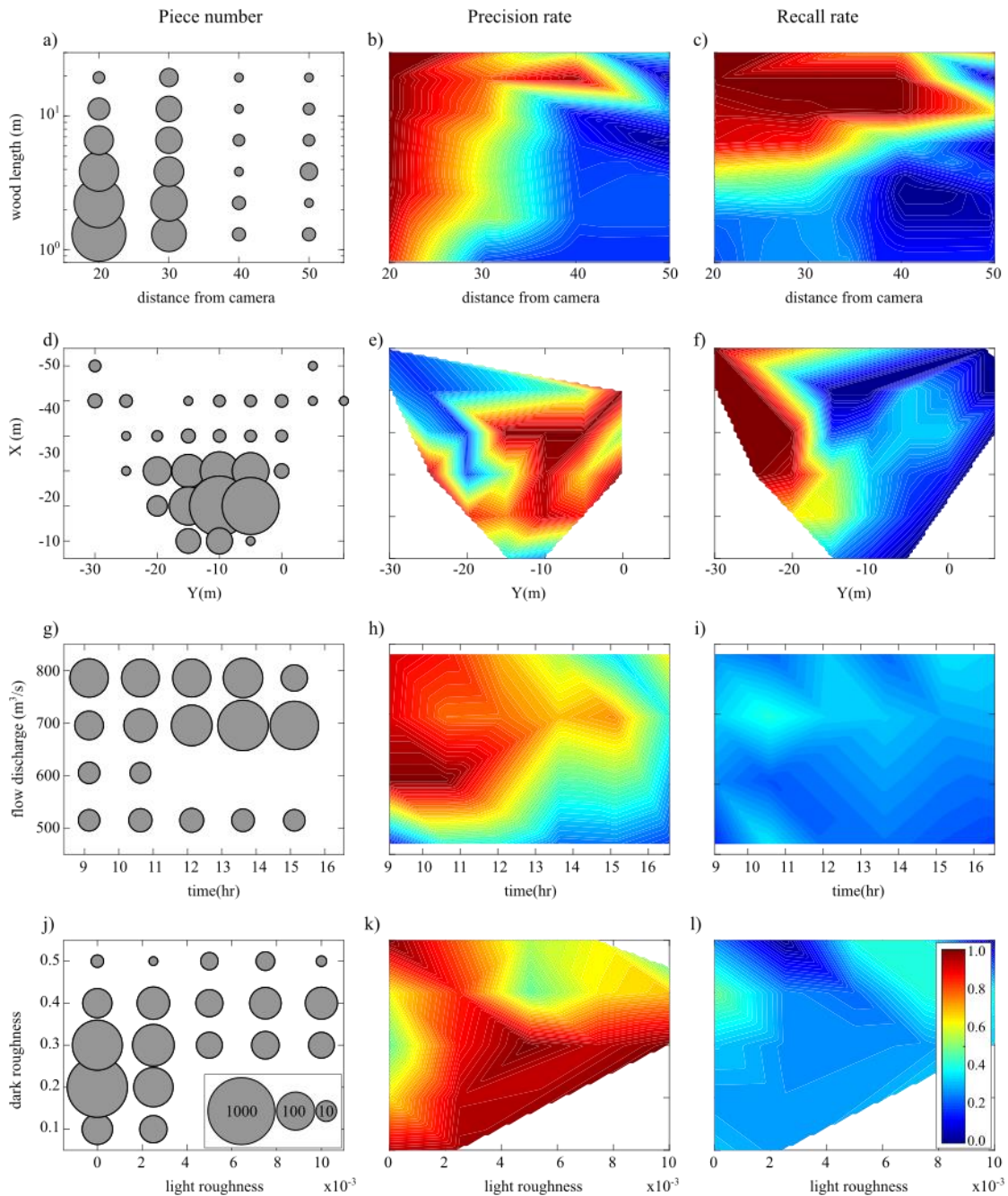
442

Fig 9 Correction matrices: a, b, c) wood lengths as a function of the distance from the camera, d, e, f) detection position, g, h, i) flow discharges during the daytime, and j, k, l) light and dark roughness's. The first column shows number of all annotated pieces. Second and third columns show Precision and Recall rates of the software respectively.

443   The presentation of model performance by pairs of correlated parameters clarifies certain strengths and
444   weaknesses of the software (Fig 9). As expected, the results of Fig 9.b indicate that first, the software is not
445   so precise for small pieces of wood (less than the order of 1 m), and second there is an obvious link between
446   wood length and the distance from the camera so that by increasing the distance from the camera, the software
447   is precise only for larger pieces of wood. Based on Fig 9.e, the software precision is usually better on the
448   right side of the frame than the left side. This spatial gradient in precision is likely because the software
449   requires an object to be detected in at least 5 continuous frames for it to be recognized as a piece of wood
450   (see Sect 3.2 and Fig 5 for more information), which means that most of the true positives are on the right
451   side of the frame where 5 continuous frames have already established. Also, the presence of the bridge pier
452   (at X $\cong$ -30 to -40 m based on Fig 9.e) in the upstream, produces lots of waves that decreases the precision
453   of the software. Also, Fig 9.h shows that the software is much more precise during the morning when there
454   is enough light rather than evening when the sunshine decreases. However, at low flow ($Q < 550\ m^3/s$) the
455   software precision decreases significantly. Finally, based on Fig 9.k, the software does not work well in two
456   roughness conditions: (i) in a dark smooth flow (light roughness $\cong 0$) when there are some dark patches
457   (shadows) on the surface (dark roughness $\cong 0.3$), and (ii) when both roughness increases and there are many
458   noises in a frame (see Fig 8).

459   To estimate the fraction of wood pieces that the software did not detect, the recall rate RR is calculated
460   in different conditions and a linear interpolation was applied on RR as it is presented in Fig 9, third column.
461   According to Fig 9.c, RR is fully dependent on piece length so that for the lengths at the order of 10 m ($L =$
462    $O(10)$) RR is very good. By contrast when $L = O(0.1{\sim}1)$ the RR is too small. There is a transient region
463   when $L = O(1)$ which is slightly depends on the distance from the camera. One can say, the wood length is
464   the most crucial parameter that affects the recall rate independent of the operator annotation. Based on Fig
465   9.f, the RR is much better on the left side of the frame than on the right side. It can be because the operator's
466   eye needs some time to detect a piece of wood, so most of the annotations are on the right side of the frame.
467   Having a small number of detections on the left side of the frame results in the small value of FN which
468   followed by high values of RR in this region ($RR = TP/(TP + FN)$). Therefore, while the position of detec-
469   tion plays a significant role in the recall rate, it is completely dependent on the operator bias. By contrast,
470   frame roughness, daytime, and flow discharge do not play a significant role in the recall rate (Fig 9. i, l).

471   **5.3. Post-processing**

472   This section is separated into two main parts. First, we show how to improve the precision of the

473   software by a posteriori distinction between TP and FP. After removing FPs from the detected pieces, in the

474   second part, we test a process to predict the annotated data that the software missed *i.e.,* false negatives.

5.3.1.   Precision improvement

476   To improve the precision of the automatic wood detection we first ran the software to detect pieces and

477   extracted the eight key parameters for each piece as described in section 5.1. Having the value of the eight

478   key parameters (four pairs of parameters in Fig 9) for each piece of wood, we then estimated the total preci-

479   sion of each object, as the average of four precisions from each sub-figure of Fig 9. In the current study the

480   detected piece was considered to be a true positive if the total precision exceeded 50%. To check the validity

481   of this process, we used cross-validation by leaving one day out, calculating the precision matrices based on

482   five other days, and applying the calculated PR matrices on the day that was left out. As is seen in Table 5,

483   this post-processing step increases the precision of the software to 85%, an enhancement of 21%. The degree

484   to which the precision is improved is dependent on the day left out for cross-validation. If, for example, the

485   day left out had similar conditions to the mean, the PR matrices were well trained and were able to distinguish

486   between TP and FP (*e.g.,* 2nd Jan with 42% enhancement). On the other hand, if we have an event with new

487   characteristics (*e.g.,* very dark and cloudy weather or at discharges different from what we have in our data-

488   base), the PR matrices were relatively blind and offered little improvement (*e.g.,* 15th Dec with 10% enhance-

489   ment).

Table 5 Precision rate (PR) before and after post-processing

		1 Jan	2 Jan	4 Jan	6 Jan	7 Jan	15 Dec	Total
Raw data	TP	745	196	31	206	29	363	1570
	FP	227	184	127	178	44	140	900
	FN	1537	606	109	506	88	933	3779
	$PR\%$	77	52	20	54	40	72	64
	$RR\%$	33	24	22	29	25	28	29
Post-proc.	TP	658	150	30	178	22	315	1353
	FP	64	10	60	39	11	68	252
	FN_{pp}[1]	87	46	1	28	7	48	217
	$PR\%$	91	94	33	82	67	82	85
	RR_{pp}[2]$\%$	88	77	97	86	76	87	86
PR improvement %		14	42	13	28	27	10	21

490   [1] FN_{pp} denotes the false estimations of the precision matrices which results in missing some TP.

491   [2] RR_{pp} denotes the recall rate of post processing which corresponds to FN_{pp}.

492   One difficulty with the post-processing reclassification of wood piece is that this new step can also
493 introduce error by classifying real objects as false positives (making them a false negative) or vice-versa.
494 Using the training data, we were able to quantify this error and categorized them as post-processed false
495 negatives ($\boldsymbol{FN_{pp}}$) with an associated recall rate ($\boldsymbol{RR_{pp}}$). As shown in Table 5, the precision enhancement
496 process lost only around 14% of TPs (RR_{pp}= 86%).

497   **5.3.2. Estimating missed wood pieces based on the recall rate**

498   The automated software detected 29% of the number of manually annotated wood pieces (Table 5). In
499 the previous section, methods were described that enhance the precision of the software by ensuring that
500 these automatically detected pieces are TPs. The larger question, however, is how to estimate the missing
501 pieces. Based on Fig 9, both PR and RR are much higher for very large objects in most areas of the image
502 and in most lighting conditions. However, the smaller pieces were found to be harder to detect, making the
503 wood length the most important factor governing the recall rate. Based on this idea, the final step in the post
504 processing is to estimate smaller wood pieces that were not detected by the software using the length distri-
505 bution extracted by the annotations.

506   The estimation is based on the concept of a threshold piece length. Above the threshold, wood pieces
507 are likely to be accurately counted using the automatic software. Below the threshold, on the other hand, the

508 automatic detection software is likely to deviate from the manual counts. The length distribution obtained

509 from the manual annotations $(TP + FN)$ (Fig 10.a) was assumed to be the most realistic distribution that can

510 be estimated from the video monitoring technique, and it was therefore used as the benchmark. Also shown

511 are the raw results of the automatic detection software $(TP + FP)$ and the raw results with the false positives

512 removed (TP). At this stage, the difference between the TP and the $TP + FN$ lines are the false negatives

513 (FN) that the software has missed. Comparison between the two lines shows that they tend to deviate between

514 2-3 m. The correlation coefficient between the length distribution of TP as one vector and $TP + FN$ as the

515 other vector was calculated for thresholds varying from 1 cm to 15 m length and 2.5 m length was defined as

516 the optimum threshold length for recall estimation (Fig 10.b).

517   In the next step we wanted to estimate the pieces less than 2.5 m that the software missed. During the

518 automatic detection process, when the software detects a piece of wood, according to Fig 9 (third column),

519 the RR can be calculated for this piece (same protocol as precision enhancement in Sect 5.3.1). Therefore, if

520 for example the average recall rate for a piece of wood is 50%, there is likely to be another piece in the same

521 condition (defined by the eight different parameters described in Table 2) that the software could not detect.

522 To correct for these missed pieces, additional pieces were added to the database, note that these pieces were

523 imaginary pieces inferred from the wood length distribution and were not detected by the software. Fig 10.a,

524 shows the length distribution after adding these virtual pieces to the database (blue line, total of 5841 pieces).

525 The result shows a good agreement between this and the operator annotations (green line, total of 6249

526 pieces), which results in a relative error of only 6.5% in the total number of wood pieces.
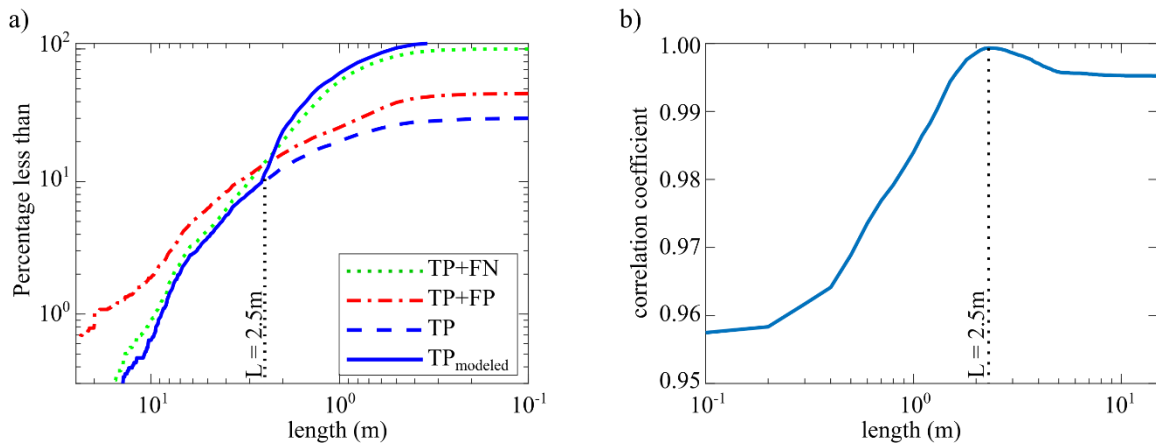
527

Fig 10 a) Steps to post-process software automatic detections: (i) raw detections ($TP + FP$ red line), (ii) Only true positives using the PR improvement process (TP blue dashed line), and (iii) modeling false negatives (blue line). Operator annotation (green dotted line is used as a benchmark). b) The correlation coefficient between operator

annotation and modeled TP to find an optimum threshold length for RR improvement.

528   On the Ain River by separating videos to 15 min segments, MacVicar and Piégay, (2012) and Zhang et

529   al. (2021) proposed the following equation for calculating wood discharge from the wood flux:

530       $$Q_w = 0.0086F^{1.24} \tag{1}$$

531   where, Q_w is the wood discharge ($m^3/15min$) and F is the wood flux (piece number/15 min). Using

532   this equation, the total volume of wood was calculated based on three different conditions: (i) operator anno-

533   tation ($TP + FN$), (ii) raw data of the detection software ($TP + FP$) and (iii) post-processed data of the de-

534   tection software ($TP_{modeled}$). Fig 11 shows a comparison of the total volume of wood from the manual an-

535   notations in comparison with the raw and post-processed annotations from the detection software. As shown,

536   the raw detection results underestimate wood volume by almost one order of magnitude. After processing,

537   the results show some scatter but are distributed around the 1:1 slope, which indicates that they follow the

538   manual annotation results. There is a slight difference for days with lower fluxes (Jan 4 and 7), where the

539   post-processing tends to over-estimate wood volumes, but in terms of an overall wood balance the volume

540   of wood on these days are negligible. In total, 125 m^3 wood was annotated by the operator and the software

541   automatically detected only 46 m^3, some of which represent false positives. After post-processing, 142 m^3

542   wood was estimated to have passed in the analyzed videos for a total error of 13.5%.
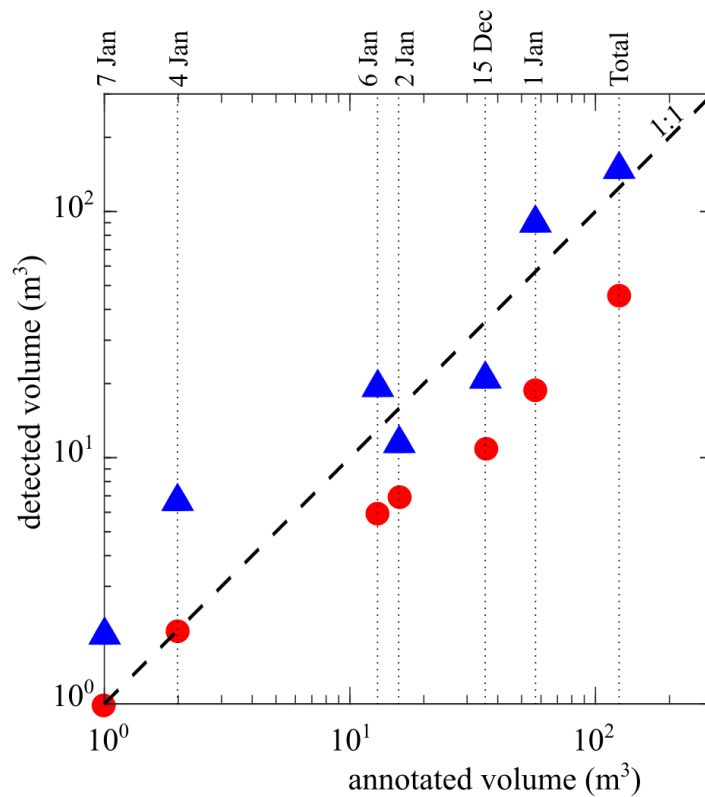
543

Fig 11 Comparison of the total volume of wood between operator annotation as the benchmark and raw data (red circles) and post-processed data (blue triangles), compared with a 1:1 line.

6.   Conclusion

Here, we present new software for the automatic detection of wood pieces on the river surface. After presenting the corresponding algorithm and the user interface, an example of automatic detection was presented. We annotated 6 days of flood events that were used to first check the performance of the software and then develop post-processing steps to both remove possibly erroneous data and model data that were possibly missed by the software. To evaluate the performance of the software, we used precision and recall rates. The automatic detection software detects around one third of all annotated wood pieces with 64% precision rate. Then using the operator annotations as the ultimate goal, the post-processing part was applied to extrapolate data extracted from detection results, aiming to come as close as possible to the annotations. It is shown that using four pair of key factors: (i) light and dark roughness of the frame, (ii) daytime and flow discharge, (iii) X, Y coordinates of detection position, and (iv) distance of detection as a function of piece

length, it is possible to detect false positives and increase the software precision to 86%. Using the concept of a threshold piece length for detection it is shown that it is then possible to model the missed wood pieces (false negatives). In the presented results, the final recall rate results in a relative error of only 6.5% for piece number and 13.5% for wood volume. It should be noted that the software cannot distinguish between a single piece of wood or the pieces in a cluster of wood in the congested wood fluxes.

This work shows the feasibility of the detection software to detect wood pieces automatically. Automation will significantly reduce the time and expertise required for manual annotation, making video monitoring a powerful tool for researchers and river managers to quantify the amount of wood in rivers. Therefore, the developed algorithm can be used to characterize wood pieces for a large image database at the study site. The results from the current study were all taken from a single site in which a large database of manual annotations was available for developing the correction procedures. In future applications it is unlikely that such a large database would be available. In such cases it is recommended to first ensure that the images collected are of high quality by following the recommendations in (Ghaffarian et al., 2020; Zhang et al., 2021). As data are collected, the automatic algorithm can be run to identify periods of high wood flux. Manual review of other high-water periods is also recommended to assess whether lighting conditions were preventing the detection of wood. When suitable flood periods with floating wood are identified, manual annotations should be done to create the correction matrices. Future applications of this approach at a wide range of sites should lead to new insights on the variability of wood pieces at the reach and watershed scales in world rivers.

Finally, we think of this work as a first step towards more autonomous systems to detect and quantify wood in rivers. Applying the post-process steps in real time is a realistic next step, because after we extract the correction matrices, which is a time-consuming process, the calculation time for PR, RR enhancement is negligible (less than 0.001s/piece). Moreover, over recent years, automatic visual recognition tasks have progressed very importantly with the advances in machine learning techniques and especially Deep Convolutional Neural Networks (DCNNs) that are now able to answer complex problems in real time. However, our context is very challenging for this class of solution, since wood objects have a highly variable shape, and they are feature in very noisy environments and a high variety of lighting conditions. Most training techniques are supervised, meaning that to train an effective DCNN to solve this problem, we would require an extensive annotated dataset. The solution presented in this work can be used as a first step towards this solution. It can be used to help human operators to quickly build annotated dataset, by correcting its output rather than annotating from scratch.

7. Code/Data/Sample availability

Not available.

8. Author contribution

Hossein Ghaffarian: Application of statistical, and computational techniques to analyses study data. Creation and presentation of the published work.

Hervé Piégay, Bruce MacVicar, Hossein Ghaffarian: Development and design of methodology; creation of models.

Laure Tougne, Pierre Lemaire: Programming and software development.

Pierre Lemaire, Zhang Zhi: Performing the surveys, and data collection.

Hervé Piégay, Bruce MacVicar, Pierre Lemaire, Hossein Ghaffarian: Critical review, commentary, and revision.

Hervé Piégay: Oversight and leadership responsibility for the research activity planning and execution, including mentorship external to the core team.

9. Competing interests

The authors declare that they have no conflict of interest.

10. Acknowledgment

This work was performed within the framework and with the support of the PEPS (RiskBof Project (2016)) and LABEX IMU (ANR-10-LABX-0088) and within the framework of the EUR H2O'Lyon (ANR-17-EURE-0018) of Université de Lyon, le latter being both part of the program "Investissements d'Avenir" (ANR-11-IDEX-0007) operated by the French National Research Agency (ANR).

11. References

Abbe TB, Montgomery DR. 2003. Patterns and processes of wood debris accumulation in the Queets river basin, Washington. Geomorphology **51** : 81–107. DOI: 10.1016/S0169-555X(02)00326-4

Ali I, Mille J, Tougne L. 2011. Wood detection and tracking in videos of rivers. 646–655 pp.

Ali I, Mille J, Tougne L. 2012. Space–time spectral model for object detection in dynamic textured background. Pattern Recognition Letters **33** : 1710–1716.

Ali I, Mille J, Tougne L. 2014. Adding a rigid motion model to foreground detection: application to moving object detection in rivers. Pattern Analysis and Applications **17** : 567–585.

Ali I, Tougne L. 2009. Unsupervised Video Analysis for Counting of Wood in River during Floods. In Advances in Visual Computing , Bebis G et al. (eds). Springer Berlin Heidelberg: Berlin, Heidelberg; 578–587. [online] Available from: http://link.springer.com/10.1007/978-3-642-10520-3_55 (Accessed 2 March 2020)

Badoux A, Andres N, Turowski JM. 2014. Damage costs due to bedload transport processes in Switzerland. Nat. Hazards Earth Syst. Sci. : 17.

Benacchio V, Piégay H, Buffin-Bélanger T, Vaudor L. 2017. A new methodology for monitoring wood fluxes in rivers using a ground camera: Potential and limits. Geomorphology **279** : 44–58. DOI: 10.1016/j.geomorph.2016.07.019

Benacchio V, Piégay H, Buffin-Belanger T, Vaudor L, Michel K. 2015. Automatioc imagery analysis to monitor wood flux in rivers (Rhône River, France)

Boivin M, Buffin-Bélanger T, Piégay H. 2015. The raft of the Saint-Jean River, Gaspé (Québec, Canada): A dynamic feature trapping most of the wood transported from the catchment. Geomorphology **231** : 270–280. DOI: 10.1016/j.geomorph.2014.12.015

Boivin M, Buffin-Bélanger T, Piégay H. 2017. Interannual kinetics (2010–2013) of large wood in a river corridor exposed to a 50-year flood event and fluvial ice dynamics. Geomorphology **279** : 59–73. DOI: 10.1016/j.geomorph.2016.07.010

630   Braudrick CA, Grant GE. 2000. When do logs move in rivers? Water Resources Research **36** : 571–
631   583. DOI: 10.1029/1999WR900290

632   Cerutti G, Tougne L, Mille J, Vacavant A, Coquin D. 2013. Understanding leaves in natural images–a
633   model-based approach for tree species identification. Computer Vision and Image Understanding **117** : 1482–
634   1501.

635   Cerutti G, Tougne L, Vacavant A, Coquin D. 2011. A parametric active polygon for leaf segmentation
636   and shape estimation. 202–213 pp.

637   Comiti F, Andreoli A, Lenzi MA, Mao L. 2006. Spatial density and characteristics of woody debris in
638   five mountain rivers of the Dolomites (Italian Alps). Geomorphology **78** : 44–63.

639   ComputerVisionToolboxTM. Release 2017b. The MathWorks, Inc., Natick, Massachusetts, United
640   States.

641   De Cicco PN, Paris E, Ruiz-Villanueva V, Solari L, Stoffel M. 2018. In-channel wood-related hazards
642   at bridges: A review: In-channel wood-related hazards at bridges: A review. River Research and Applications
643   **34** : 617–628. DOI: 10.1002/rra.3300

644   Forsyth D, Ponce J. 2012. Computer vision: a modern approach . 2nd ed. Pearson: Boston

645   Ghaffarian H, Piégay H, Lopez D, Rivière N, MacVicar B, Antonio A, Mignot E. 2020. Video-moni-
646   toring of wood discharge: first inter-basin comparison and recommendations to install video cameras. Earth
647   Surface Processes and Landforms **45** : 2219–2234. DOI: https://doi.org/10.1002/esp.4875

648   Gordo A, Almazán J, Revaud J, Larlus D. 2016. Deep image retrieval: Learning global representations
649   for image search. 241–257 pp.

650   Gregory S, Boyer KL, Gurnell AM. 2003. Ecology and management of wood in world rivers

651   Gurnell AM, Piégay H, Swanson FJ, Gregory SV. 2002. Large wood and fluvial processes. Freshwater
652   Biology **47** : 601–619. DOI: 10.1046/j.1365-2427.2002.00916.x

653   Haga H, Kumagai T, Otsuki K, Ogawa S. 2002. Transport and retention of coarse woody debris in

654 mountain streams: An in situ field experiment of log transport and a field survey of coarse woody debris

655 distribution: COARSE WOODY DEBRIS IN MOUNTAIN STREAMS. Water Resources Research **38** : 1-

656 1-1–16. DOI: 10.1029/2001WR001123

657 Jacobson PJ, Jacobson KM, Angermeier PL, Cherry DS. 1999. Transport, retention, and ecological sig-

658 nificance of woody debris within a large ephemeral river. Journal of the North American Benthological So-

659 ciety **18** : 429–444.

660 Keller EA, Swanson FJ. 1979. Effects of large organic material on channel form and fluvial processes.

661 Earth Surface Processes **4** : 361–380. DOI: 10.1002/esp.3290040406

662 Kramer N, Wohl E. 2014. Estimating fluvial wood discharge using time-lapse photography with varying

663 sampling intervals. Earth Surface Processes and Landforms **39** : 844–852.

664 Kramer N, Wohl E, Hess-Homeier B, Leisz S. 2017. The pulse of driftwood export from a very large

665 forested river basin over multiple time scales, Slave River, Canada. Water Resources Research **53** : 1928–

666 1947.

667 Lagasse PF. 2010. Effects of debris on bridge pier scour . Transportation Research Board

668 Lassettre NS, Piégay H, Dufour S, Rollet A-J. 2008. Decadal changes in distribution and frequency of

669 wood in a free meandering river, the Ain River, France. Earth Surface Processes and Landforms **33** : 1098–

670 1112. DOI: 10.1002/esp.1605

671 Lejot J, Delacourt C, Piégay H, Fournier T, Trémélo M-L, Allemand P. 2007. Very high spatial resolu-

672 tion imagery for channel bathymetry and topography from an unmanned mapping controlled platform. Earth

673 Surface Processes and Landforms: The Journal of the British Geomorphological Research Group **32** : 1705–

674 1725.

675 Lemaire P, Piegay H, MacVicar B, Mouquet-Noppe C, Tougne L. 2014. Automatically monitoring

676 driftwood in large rivers: preliminary results

677 Lienkaemper GW, Swanson FJ. 1987. Dynamics of large woody debris in streams in old-growth Doug-

678 las-fir forests. Canadian Journal of Forest Research **17** : 150–156.

679  Liu L, Ouyang W, Wang X, Fieguth P, Chen J, Liu X, Pietikäinen M. 2020. Deep learning for generic
680 object detection: A survey. International journal of computer vision **128** : 261–318.

681  Lucía A, Comiti F, Borga M, Cavalli M, Marchi L. 2015. Dynamics of large wood during a flash flood
682 in two mountain catchments. Natural Hazards and Earth System Sciences **15** : 1741.

683  Lyn D, Cooper T, Yi Y-K. 2003. Debris accumulation at bridge crossings: laboratory and field studies
684 . Purdue University: West Lafayette, IN [online] Available from: http://docs.lib.purdue.edu/jtrp/48 (Accessed
685 2 March 2020)

686  MacVicar B, Piégay H. 2012. Implementation and validation of video monitoring for wood budgeting
687 in a wandering piedmont river, the Ain River (France). Earth Surface Processes and Landforms **37** : 1272–
688 1289. DOI: 10.1002/esp.3240

689  MacVicar BJ, Piégay H, Henderson A, Comiti F, Oberlin C, Pecorari E. 2009a. Quantifying the tem-
690 poral dynamics of wood in large rivers: field trials of wood surveying, dating, tracking, and monitoring tech-
691 niques. Earth Surface Processes and Landforms **34** : 2031–2046. DOI: 10.1002/esp.1888

692  MacVicar BJ, Piégay H, Tougne L, Ali I. 2009b. Video monitoring of wood transport in a free-mean-
693 dering piedmont river. AGUFM **2009** : H54A-05.

694  Mao L, Comiti F. 2010. The effects of large wood elements during an extreme flood in a small tropical
695 basin of Costa Rica. WIT Transactions on Engineering Sciences **67** : 225–236.

696  Marcus WA, Legleiter CJ, Aspinall RJ, Boardman JW, Crabtree RL. 2003. High spatial resolution hy-
697 perspectral mapping of in-stream habitats, depths, and woody debris in mountain streams. Geomorphology
698 **55** : 363–380.

699  Marcus WA, Marston RA, Colvard Jr CR, Gray RD. 2002. Mapping the spatial and temporal distribu-
700 tions of woody debris in streams of the Greater Yellowstone Ecosystem, USA. Geomorphology **44** : 323–
701 335.

702  Martin DJ, Benda LE. 2001. Patterns of Instream Wood Recruitment and Transport at the Watershed
703 Scale. Transactions of the American Fisheries Society **130** : 940–958. DOI: 10.1577/1548-

704   8659(2001)130<0940:POIWRA>2.0.CO;2

705   Mazzorana B, Ruiz-Villanueva V, Marchi L, Cavalli M, Gems B, Gschnitzer T, Mao L, Iroumé A,
706   Valdebenito G. 2018. Assessing and mitigating large wood-related hazards in mountain streams: recent ap-
707   proaches: Assessing and mitigating LW-related hazards in mountain streams. Journal of Flood Risk Manage-
708   ment **11** : 207–222. DOI: 10.1111/jfr3.12316

709   Moulin B, Piegay H. 2004. Characteristics and temporal variability of large woody debris trapped in a
710   reservoir on the River Rhone(Rhone): implications for river basin management. River Research and Appli-
711   cations **20** : 79–97. DOI: 10.1002/rra.724

712   Muste M, Fujita I, Hauet A. 2008. Large-scale particle image velocimetry for measurements in riverine
713   environments. Water resources research **44** : W00D19.

714   Piegay H, Lemaire P, MacVicar B, Mouquet-Noppe C, Tougne L. 2014. Automatically monitoring
715   driftwood in large rivers: preliminary results. AGUFM **2014** : EP53D-3695.

716   Ravazzolo D, Mao L, Picco L, Lenzi MA. 2015. Tracking log displacement during floods in the Taglia-
717   mento River using RFID and GPS tracker devices. Geomorphology **228** : 226–233. DOI: 10.1016/j.geo-
718   morph.2014.09.012

719   Roussillon T, Piégay H, Sivignon I, Tougne L, Lavigne F. 2009. Automatic computation of pebble
720   roundness using digital imagery and discrete geometry. Computers & Geosciences **35** : 1992–2000.

721   Ruiz-Villanueva V et al. 2019. Characterization of wood-laden flows in rivers: wood-laden flows. Earth
722   Surface Processes and Landforms **44** : 1694–1709. DOI: 10.1002/esp.4603

723   Ruiz-Villanueva V, Bodoque JM, Díez-Herrero A, Bladé E. 2014. Large wood transport as significant
724   influence on flood risk in a mountain village. Natural hazards **74** : 967–987.

725   Ruiz-Villanueva V, Piégay H, Gurnell AM, Marston RA, Stoffel M. 2016. Recent advances quantifying
726   the large wood dynamics in river basins: New methods and remaining challenges: Large Wood Dynamics.
727   Reviews of Geophysics **54** : 611–652. DOI: 10.1002/2015RG000514

728   Schenk ER, Moulin B, Hupp CR, Richter JM. 2014. Large wood budget and transport dynamics on a

large river using radio telemetry. Earth Surface Processes and Landforms **39** : 487–498. DOI: 10.1002/esp.3463

Senter A, Pasternack G, Piégay H, Vaughan M. 2017. Wood export prediction at the watershed scale. Earth Surface Processes and Landforms **42** : 2377–2392. DOI: 10.1002/esp.4190

Senter AE, Pasternack GB. 2011. Large wood aids spawning Chinook salmon (Oncorhynchus tshawytscha) in marginal habitat on a regulated river in California. River Research and Applications **27** : 550–565.

Seo JI, Nakamura F. 2009. Scale-dependent controls upon the fluvial export of large wood from river catchments. Earth Surface Processes and Landforms **34** : 786–800. DOI: 10.1002/esp.1765

Seo JI, Nakamura F, Chun KW. 2010. Dynamics of large wood at the watershed scale: a perspective on current research limits and future directions. Landscape and Ecological Engineering **6** : 271–287.

Seo JI, Nakamura F, Nakano D, Ichiyanagi H, Chun KW. 2008. Factors controlling the fluvial export of large woody debris, and its contribution to organic carbon budgets at watershed scales. Water Resources Research **44**

Turowski JM, Badoux A, Bunte K, Rickli C, Federspiel N, Jochner M. 2013. The mass distribution of coarse particulate organic matter exported from an Alpine headwater stream. Earth surface dynamics **1** : 1–11.

Viola PA, Jones MJ. 2006. Object recognition system

Warren DR, Kraft CE. 2008. Dynamics of large wood in an eastern US mountain stream. Forest Ecology and Management **256** : 808–814.

Wohl E. 2013. Floodplains and wood. Earth-Science Reviews **123** : 194–212.

Wohl E, Scott DN. 2017. Wood and sediment storage and dynamics in river corridors. Earth Surface Processes and Landforms **42** : 5–23.

Zhang Z, Ghaffarian H, MacVicar B, Vaudor L, Antonio A, Michel K, Piégay H. 2021. Video

753   monitoring of in-channel wood: From flux characterization and prediction to recommendations to equip sta-

754   tions. Earth Surface Processes and Landforms **n/a** DOI: 10.1002/esp.5068 [online] Available from:

755   https://onlinelibrary.wiley.com/doi/abs/10.1002/esp.5068 (Accessed 9 February 2021)

756